Ph.D. THESIS

FATTY LIVER, OBESITY AND HEPATOCELLULAR CANCER: IMPACTS OF UNCOUPLING PROTEIN-2 AND FLUVASTATIN

Péter Fülöp, M.D.

Supervisors:

György Paragh, M.D., D.Sc.

György Baffy, M.D., Ph.D.

UNIVERSITY OF DEBRECEN

MEDICAL AND HEALTH SCIENCE CENTER

1ST DEPARTMENT OF MEDICINE

2007

1. INTRODUCTION

1.1. Non-alcoholic fatty liver

Obesity and its associated co-morbidities are among the most prevalent and challenging conditions that confront the medical profession in the 21st century. A major metabolic consequence of obesity is insulin resistance, which is associated with the deposition of triglycerides in the liver. Resulting in hepatic steatosis, the non-alcoholic fatty liver disease (NAFLD) is the most frequent manifestation of liver diseases in the developed civilizations. NAFLD is a clinicopathological term that encompasses a disease spectrum from simple triglyceride accumulation to hepatic steatosis with inflammation (non-alcoholic steatohepatitis, NASH), fibrosis, cirrhosis (cryptogenic cirrhosis) and – ultimately – hepatocellular cancer (HCC). Besides the potential progressivity its clinical importance can be accentuated by its prevalence: NAFLD is the most common cause of abnormal liver function tests in the United States. The prevalence of NAFLD in the general population is estimated to be between 10% and 24%; while NASH is present in 2-3% of the population. Non-alcoholic fatty liver is a common hepatic manifestation of metabolic disorders that are characterized by obesity, hyperinsulinemia, insulin resistance and hypertriglyceridemia. Therefore, NAFLD is a feature of metabolic syndrome. The pathogenesis of the disease is incompletely understood, however, it is increasingly recognized that hepatic lipid peroxidation, adenozin triphosphate (ATP) depletion and dysfunction of Kupffer cells and mitochondria are involved in the disease manifestation. Day and James initially proposed a ”two-hit” model to explain the progression of NAFLD. The ”first hit” constitutes the deposition of triglycerides in the cytoplasm of the hepatocytes accompanying the evolution of insulin resistance. Triglycerid accumulation developing on the surfeit of the β oxidation in the mitochondria promotes the more progressive liver disease evolving from the increased oxidative stress as a ”second hit”.

Insulin resistance in obesity is described by hyperinsulinemia, increased glucose output and decreased glucose utilization of the liver. Increased activity of activity of hormone-sensitive lipase contributes to the excessive free fatty acid (FFA) flux into the liver. The rate of hepatic FFA uptake is unregulated and therefore directly proportional to plasma FFA concentrations. FFAs taken up by the liver are oxidized in the mitochondria to generate ATP, or undergo esterification to produce triglycerides, which are either stored within the hepatocye or incorporated into very low density lipoprotein (VLDL) particles for secretion. Independently from each other, but acting synergistically, insulin and glucose increase fatty acid production from excess glucose with the help of transcription factors (sterol regulatory element-binding protein-1c: SREBP-1c; and carbohydrate response element binding protein: ChREBP). The third transcription factor that participates in the development of steatosis is peroxisome proliferator activator receptor-γ (PPARγ). In animal models of insulin resistance and fatty livers, its expression is markedly increased, however the mechanism for promoting hepatic triglyceride accumulation is yet to be cleared. Increased lipogenesis and triglyceride synthesis

results in exaggerated production of malonyl-CoA, which inhibits the activity of carnitine palmitoyl transferase-1 (CPT-1) and fatty acid entry into the mitochondria, thus reducing β oxidation and enhancing fatty acid and triglyceride accumulation.

1.2. Non-alcoholic steatohepatitis

Oxidative stress results from the imbalance between pro-oxidant and antioxidant factors. The predominant pro-oxidant chemicals in fatty liver are singlet oxygen molecules, superoxide anions, hydrogen peroxide, and hydroxyl radicals: molecules collectively referred to as reactive oxygen species (ROS). Fatty acid oxidation is a major source of cellular ROS generation: mitochondrial β oxidation through the electron transport chain (ETC), peroxisomal β oxidation via the acyl-CoA oxidase (AOX), and microsomal ω oxidation with the help of the cytochrome P450 system collectively contribute to oxidative stress. Polyunsaturated fatty acids (PUFAs) are extremely susceptible to lipid peroxidation generated by ROS, which results in the formation of aldehyde by-products such as hydroxynonenal (HNE) and malondialdehyde (MDA). These molecules are toxic by themselves, and can freely diffuse into the extracellular space to harm distant cells. Reactive oxygen species and toxic aldehydes cause depletion of ATP and nicotinamide dinucleotide, DNA damage, protein denaturation, glutathione depletion and membrane destruction resulting in increased oxidative stress and cell death. Also, they promote the secretion of proinflammatory cytokines and neutrophil chemotaxis and lead to fibrosis by activating the collagen producing hepatic stellate cells (HSCs). Human livers with NASH have increased levels of by-products of lipid peroxidation.

Mitochondrial dysfunction is also prevalent in non-alcoholic steatohepatitis. Ultrastructural mitochondrial abnormalities have been documented in NASH that are indicative of defective oxidative phosphorylation and curbed ETC activity, together with ATP depletion. If the electron flow is interrupted at any point in the electron transport chain, the preceeding respiratory intermediates can transfer electrons to molecular oxygen to produce superoxide anions and hydrogen peroxide. As the oxidative capacity of the mitochondria becomes impaired, cytosolic fatty acids accumulate. Alternative fatty acid oxidation pathways in the peroxysomes and in microsomes are activated, resulting in the formation of additional ROS. Attacking fatty acids localized in the mitochondrial membrane, HNE and MDA additionally worsen the electron transport and enhance the proteolysis of apolipoprotein B (ApoB), thereby attenuating VLDL secretion. The reduction in VLDL secretion may further contribute to triglyceride accumulation in the liver. Steatosis is accompanied by chronic inflammation in the liver of obese rodents, and is characterized by increased activity of hepatic NF-κB (nuclear factor kappa B), resulting in elevated levels of some cytokines, such as tumor necrosis factor alpha (TNF-α), interleukin-6 and -1β (IL-6, IL-1β). Cytokines activate Kupffer cells and participate in all typical features of NASH, such as hepatocyte necrosis and apoptosis, neutrophil chemotaxis, HSC activation and Mallory body formation.

1.3. The uncoupling protein-2 (UCP2)

Uncoupling (i.e., disconnection of ATP synthesis from proton gradient built up around the mitochondrial inner membrane) has long been a tempting target in the treatment of obesity. In 1961, Peter Mitchell published his milestone chemiosmotic theory about oxidative phosphorylation and mitochondrial energy production. Reducing equivalents originating from glucose and fatty acid oxidation donate electrons to the ETC. Electrons are passed along the complexes to ultimately reduce molecular oxygen to water at cytochrome c oxidase (complex IV). This series of highly exergonic reactions provides energy for the outward translocation of protons from the mitochondrial matrix into the intermembrane space to create an electrochemical gradient (mitochondrial membrane gradient; $\Delta\Psi m$) accross the inner membrane. This mitochondrial membrane potential will then drive energy synthesis through the controlled return of protons into the matrix via the ATP synthase.

It is noted, that oxidative phosphorylation is never 100% efficient, meaning that a portion of consumed oxygen – on the ground of the proton leak – is not used for ATP synthesis and dissipated as heat energy. In addition to inherent properties of the inner membrane (basal proton conductance), proton leak may result from the action of specialized carrier proteins (inducible proton conductance). Uncoupling protein (UCP or thermogenin, latter renamed UCP1), performs precisely this function in the mitochondria of brown adipose tissue, thus this protein is a key mediator of cold-induced thermogenesis.

Independently from each other, UCP2 was identified by cloning strategies in 1997 by two research groups. The *ucp2* gene was mapped to chromosome 7 in mouse and to the synthetic region 11q13 in man. UCP2 in humans is a 308 amino acid protein with molecular weight of 33 kDa and a 59% amino acid identity to UCP1. Consequently, the structure of UCP2 protein is very similar to that of UCP1 and is remarkably well conserved between different species. Akin to all members of the mitochondrial carrier family, UCP2 contains six alpha-helical spanners and is embedded in the mitochondrial inner membrane where it functions as a homodimer. The high homology with UCP1 suggested that UCP2 might also act as a modulator of thermogenesis; however, the physiological role of UCP2-mediated proton leak still remains a matter of debate. UCP2 induces proton conductance in yeast only when expressed a magnitude over the physiological concentration. UCP2 is present to some degree in virtually every mammalian tissue; however, its expression is one to two magnitudes smaller when compared to UCP1 abundance in brown adipose tissue. Consequently, contribution of UCP2 to proton leak is likely to be much more modest. It is also known, that mice deficient for UCP2 (UCP2-knockout, UCP2-KO) remain lean with no discernible effect on their basal metabolic rate.

The first studies detected UCP2 mRNA in several tissues; however, its expression was found particularly high in the components of the immune system, such as the thymus, spleen and macrophages. It was also noted, that UCP2 mRNA did not always correlate with its protein levels, showing a potential role for translational regulation. Despite its rather ubiquitious presence, expression

of UCP2 is localized mainly in the Kupffer cells of the healthy liver, with very low or undetectable levels in hepatocytes. To our recent knowledge, UCP2 has several different functions:

1. It limits the generation of reactive oxygen species,
2. It interferes with the ATP synthesis in the cells,
3. It modulates fatty acid metabolism.

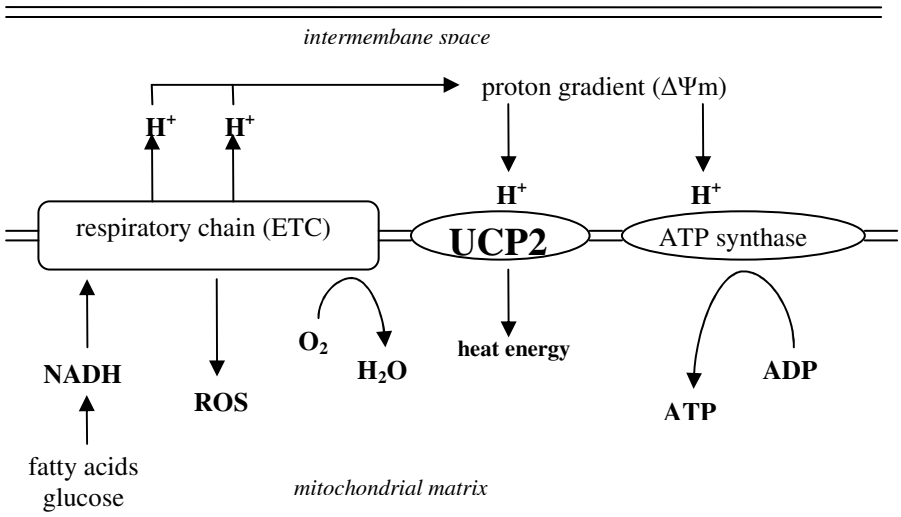

Fig. 1. Physiological effects of UCP2 in the inner mitochondrial membrane

1. UCP2 mitigates ROS generation: If large amounts of reducing equivalents are available (in cases of obesity, diabetes, or prolonged fasting), the respiratory chain slows down, resulting in depletion of adenosin diphosphate (ADP) stores with maximal ATP synthesis. Mitochondrial hyperpolarization slows ETC down and prolongs the half-life of mobile electron carriers that will mediate partial reduction of oxygen and generate superoxide. Therefore, UCP2-mediated proton leak (”mild uncoupling”) is favorable to decrease proton gradient and help the electrons to flow along the ETC undisturbedly, which results in a cutback of ROS generation. Also, a reciprocal correlation is noted between UCP2 and ROS: superoxide and its derivatives enhance UCP2 expression and proton conductance in the mitochondrial matrix.

2. UCP2 reduces ATP synthesis: If protons bypass ATP synthase and flow back to the matrix through the UCP2, the cellular ATP synthesis becomes compromised. This alternative modulation of ATP synthesis manifests in the β-cells, in which UCP2 negatively regulates insulin production

3. UCP2 modulates fatty acid metabolism: The mechanism of UCP2-mediated proton transport is still unclear, however, it is noted that UCP2 expression in hepatocytes is very small, but it shows significant upregulation in the liver during conditions associated with elevated plasma FFA

levels and steatosis, supporting the view that UCP2 participate in the pathogenesis of NAFLD. Livers of leptindeficient *ob/ob* mice showed increased UCP mRNA and protein levels when compared to lean animals. It is noted, that UCP2 functions as a proton transporter only in the presence of specific activators. Fatty acids and lipid peroxides can activate UCP2 by decreasing the inhibitory effect of purine nucleotides on the protein.

1.4. UCP2 and non-alcoholic fatty liver disease

It is presumable that UCP2 activity facilitates fatty acid oxidation, especially in cases of fuel surplus, such as obesity. In another way, flawless lipid catabolism may require the presence of operational UCP2. Its expression is localised in Kupffer cells of the healthy liver, while parenchymal cells show almost undetectable UCP2 expression with a significant increase in steatosis. Lipids accumulating in the liver are not inert, therefore they make the fatty liver more susceptible to the ”second hit”. ROS generation resulting from the enhanced fatty acid influx presents a significant toxicity to the liver tissue. It could be plausible that increased UCP2 expression protects hepatocytes from oxidative stress, however, rodent fatty livers show enhanced oxidative stress despite the significant increase in UCP2 expression. While studies that link ROS to UCP2 activation make it conceivable that UCP2 in fatty liver is not only highly expessed but also functional, there is no good evidence that UCP2 in turn would help to reduce ROS production and protect against steatohepatitis. An interesting phenomenon may answer resolve this paradox. According to this, an opposing regulation of UCP2 expression may occur in non-parenchymal and parenchymal cells during NAFLD: upregulation of UCP2 detected in the hepatocytes is associated by a concomitantly diminished UCP2 expression in Kupffer cells and other macrophages. If UCP2 really inhibits ROS formation in NASH, downregulation of UCP2 in Kupffer cells, rather than its upregulation in hepatocytes, may be a key contributor to increased oxidative stress. This negative regulation in the macrophages is proven only in response to endotoxin.

While history of obesity in cryptogenic cirrhosis is an independent predictor of HCC, obesity even without cirrhosis appears to be a risk factor for the development of cancer. Incidence of HCC is higher in *ob/ob* mice that have obesity and severe steatosis. It was suggested that not fibrosis, but insulin resistance *per se* might be the cause of HCC in NAFLD. Mitochondria occupy a central role in the regulation of apoptosis. While the intrinsic apoptosis pathway primarily responds to metabolic perturbations and intracellular oxidative stress, the extrinsic pathway is activated through cell surface death receptors (e.g., Fas/CD95). There is evidence for crosstalk between these two pathways and for mitochondrial involvement in both processes. Major apoptosis events include oligomerization of pro-apoptotic Bcl2 proteins and their translocation to the mitochondria, permeabilization of the mitochondrial outer membrane, disruption of $\Delta\Psi m$, release of intermembrane constituents (e.g., cytochrome c) into the cytosol, activation of initiator and executioner caspases, concluding into disassembly of the cell. It is known that ROS production is increased in cancer cells. Modulating

mitochondrial membrane potential, UCP2 may interfere with ROS generation and ATP production resulting in subsequent decisions on the fate of cancer cells. This suggests that cancer cells may eventually use enhanced UCP2 function to gain survival advantage.

1.5. The pleiotropic effects of statins

Treatment of hyperlipidemia, which often accompanies obesity, is essential to avoid long-term ischemic complications. Non-steroid inhibitors of 3-hydroxy-3-methylglutaryl coenzyme A (HMG-CoA) reductase, also named as statins, block the key enzyme of cholesterol biosynthesis, which results in increased expression of LDL receptors and enhanced uptake of cholesterol from the blood. Studies with statins and high subject number showed better morbidity and mortality rates than expected from lipid lowering alone. This suggests that statins have additional (so-called pleiotropic) effects beyond decreasing serum lipid levels: they improve endothelial dysfunction, inhibit platelet activation, thromboxane formation and leukocyte adhesion to the endothelium, as well as the pro-inflammatory effect of C-reactive protein (CRP). Statins have a potent antioxidant effect and stabilize atherosclerotic plaques, plus slow the progression of Alzheimer's disease.

Inhibiting HMG-CoA reductase, statins reduce the production of non-cholesterol mevalonate metabolites. These isoprenoids (farnesyl pyrophosphate and geranyl-geranyl pyrophosphate) are involved in post-translational modification (prenylation) of small guanosine triphosphate (GTP)-binding proteins (Rho, Ras) which modulate cellular signal transduction. Prenylation of small GTPases results in conformation of the active, membrane-bound protein form.

1.6. The impact of statins on tumor formation

Inhibiting cell proliferation and inducing apoptosis, statins are proved to decrease tumor growth in vivo and in vitro. Their antitumor effect is founded upon mevalonate cycle inhibition, because both farnesyl pyrophosphate and geranyl-geranyl pyrophosphate are involved in regulating cell proliferation and cell death. Isoprenoids are necessary for maturation of some proteins (laminin, G-proteins and small GTPases) and for membrane localization and subsequent activation of growth-modulatory proteins. HMG-CoA reductase inhibitors also inhibit metastasis formation. Prevalence of colon, prostate and vesical bladder cancer was shown diminished in patients receiving statins when compared to those not obtaining HMG-CoA medication. While these effects of statins are important for their clinical use, information about their effect on tumor and metastasis formation is still limited. It is also unclear, whether statins with different molecular structure act similarly on tumor growth.

1.7. About fluvastatin

Fluvastatin is a synthetic HMG-CoA reductase inhibitor with an open-ring structure that has been used for treatment of hyperlipidemia and atherosclerosis since the 1990's. It possesses an inhibitory effect on smooth muscle cell proliferation in the vessel wall and invasiveness of human

pancreas cancer cells by inhibiting RhoA-mediated geranylgeranylation. It also inhibits low-density lipoprotein (LDL) oxidation and superoxide formation.

Similarly to atorvastatin, fluvastatin is a 4-fluorophenyl molecule. It is suggested, that its antioxidant and nitrogen monoxide synthase inhibitory properties are based upon its chemical structure and lipophilic character. Fluvastatin is selective to the liver and is available in 40 and 80 mg doses in Hungary.

2. AIMS

2.1. UCP2 and acute liver injury

We asked whether absence of UCP2 protects *ob/ob* mice from Fas-mediated acute liver damage to determine the ”deleterious” effect of the protein on compromising ATP stores; and also, to evaluate the ”beneficial” effect on limiting ROS generation. Acute liver injury was initiated by intraperitoneal administration of agonistic anti-Fas antibody (Jo2) in UCP2-deficient *ob/ob* mice *(ob/ob:ucp2$^{-/-}$)* and UCP2-competent *(ob/ob:ucp2$^{+/+}$)* littermates. Jo2 treatment predictably induces death receptor–mediated hepatocellular destruction and fulminant liver failure in mice. We determined survival rates, ROS generation and ATP stores in the fatty livers of mice with different genotypes and also evaluated histological differences. Our aim was also to study cell-specific regulation of UCP2 in the development of fatty liver and its effect on acute liver injury.

2.2. Effect of fluvastatin on the development of hepatocellular cancer

We addressed this question by using implanted hepatocellular cancer cells into the renal capsule of rats. We aimed to determine the possible antitumor effect of fluvastatin on cancer cell growth to prove its pleiotropic effect. We also decided to evaluate the preventive and therapeutic anticancer effects of fluvastatin administered orally in the absence of any other anticancer drug.

3. METHODS

3.1 Animals and treatment

Heterozygous founders of ucp2 mice were obtained from Dr. Bradford Lowell (Boston, MA), crossbred with ob/ob mice (Jackson Laboratories, Bar Harbor, ME), and genotyped as previously described *(Zhang C, et al. Cell 2001; 105:745-755).* Because the availability of double homozygous offspring was much limited, 8- to 18-week-old obese female littermates of heterozygous parents that had both alleles for the ucp2 gene *(ob/ob:ucp2$^{+/+}$)* or were nullizygous for it mice *(ob/ob:ucp2$^{-/-}$)* were chosen to receive a single intraperitoneal injection of Jo2 antibody (BD PharMingen, San Diego, CA)

at low (0.15 mg/kg) or high (0.40 mg/kg) doses. Control animals were injected with saline. Serum alanine aminotransferase (ALT) levels were monitored up to 24 hours unless the mice died earlier. Blood was obtained through the tail vein or by cardiac puncture. Livers were excised and snap-frozen in liquid nitrogen or processed for histological studies. The Lifespan Animal Welfare Committee of Rhode Island Hospital, Providence, RI, approved all animal experiments.

3.2. Histological studies and image analysis

Liver tissue was fixed overnight in 4% paraformaldehyde dissolved in phosphate-buffered saline at 4°C, then dehydrated, embedded in paraffin, and cut into 4-μm thickness. Hepatocellular apoptosis and necrosis was assessed by hematoxylin-eosin staining and by use of the terminal deoxynucleotidyl transferase-mediated nick-end labeling (TUNEL) assay (ApopTag Plus Peroxidase, Serologicals Corp., Norcross, GA). Labeling indices were determined without knowledge of the genotypes by counting TUNEL-positive nuclei per 100 hepatocytes. At least 2,000 hepatocytes were counted for each animal. To assess the combined extent of apoptosis and necrosis in the liver, we prepared digitized images of TUNEL slides (MicroPublisher 3.3 RTV, Qimaging, Burnaby, British Columbia). We recorded the area and intensity of peroxidase staining above a constant optical density threshold using Image Pro Plus 5.1 (MediaCybernetics, Silver Springs, MD) to calculate and express the integrated optical density in arbitrary units. Constant optical conditions were maintained along the entire morphometric evaluation.

3.3. DNA fragmentation assay

DNA fragmentation was assessed by the accelerated apoptotic DNA laddering protocol,31 using slight modification. Briefly, liver tissue was homogenized in lysis buffer (50 mmol/L Tris-HCl, pH 7.5, 1% NP-40, 20 mmol/L EDTA). The lysate was pelleted at 16,000g (5 minutes, 4°C), and the supernatant was subject to one round of phenol:chloroform:isoamyl alcohol (25:24:1; pH 7.4; 0.5 mL) extraction. Apoptotic DNA fragments were precipitated from the liquid phase by adding 50 μL of 3 mol/L sodium acetate (pH 5.2), 1 μL nuclease-free glycogen (Roche, Mannheim, Germany) and 0.6 mL isopropanol. After incubation on ice for 5 minutes, the precipitated nucleic acids were pelleted by centrifugation at 12,900g (10 minutes, 4°C). After washing with 70% ethanol, the pellet was reconstituted in TE buffer, and the DNA concentration was measured by spectrophotometry. Equal amounts of DNA were digested with RnaseOne (Promega, Madison, WI). After digestion, 5x Orange G dye was added to each sample, and the apoptotic DNA fragments were resolved by 1.8% TAE agarose gel electrophoresis.

3.4. Biochemical assays

We used a commercially available kit to measure serum ALT levels (Infinity ALT Reagent, Sigma, St. Louis, MO). To assess generation of ROS in the liver, we measured the tissue content of

malondialdehyde (MDA), a terminal product of lipid peroxidation. Briefly, snap-frozen liver tissue was homogenized in 0.9% (w/v) saline containing 1% (v/v) butylated hydroxytoluene to determine MDA levels by a commercially available kit (Bioxytech MDA-586, OxisResearch, Portland, OR). To assess liver tissue ATP content, snap-frozen liver tissue was homogenized in a sample buffer (20 mmol/L glycine, 50 mmol/L MgSO4, 4 mmol/L EDTA, pH 7.75) and a luciferin-luciferase assay was performed (ATPLite Luminescence ATP Detection System, Perkin-Elmer Life Sciences, Boston, MA). Unless otherwise specified, all chemicals were obtained from Sigma.

3.5. Western blot analysis

Liver tissue lysates were prepared in a mixture of 30 mmol/L Tris (pH 7.5), 2 mmol/L EDTA, 150 mmol/L NaCl, 0.1% SDS, 1% NP-40, 10% glycerol, 0.5% Na-deoxycholate containing protease inhibitors (Complete Mini EDTA-free Protease Inhibitor Cocktail, Roche, Indianapolis, IN). Protein concentrations of the lysates were determined using the BCA Protein Assay Reagent Kit (Pierce Biotechnology, Rockford, IL). Protein extracts were fractionated by 10% SDS-PAGE and transferred to a nitrocellulose membrane (Perkin-Elmer). Immunoblots were performed using polyclonal rabbit antibodies (1:1,000) against the murine Fas receptor (CD95) (Abcam, Cambridge, MA). Secondary antibodies were conjugated with horseradish peroxidase and immunoblots detected by ECL (Perkin-Elmer). Equal loading was confirmed using betaactin antibody.

3.6. Liver perfusion and cell separation

Parenchymal cells (PC) and nonparenchymal cells (NPC) were isolated from the livers of 8- to 12-week-old UCP2-competent *ob/ob* mice and their lean *(wt/wt)* littermates, by a modified two-step in situ collagenase perfusion method from Van Harken. Briefly, the animals were anesthetized, laparotomy was performed, the portal vein was cannulated and perfused for 10 minutes with Krebs-Ringer buffer (KRB; containing 20 mmol/L glucose and 0.1 mmol/L EGTA), followed by perfusion for an additional 10 minutes with KRB (supplemented with 20 mmol/L glucose, 1.37 mmol/L CaCl2, and 150 U/mL type I collagenase, Worthington, Lakewood, NJ) at a flow rate of 2 to 3 mL/min. To obtain PC fraction, the livers were removed from the carcass, minced, filtered through a 70-μm cell strainer (BD Falcon, San Jose, CA), and centrifuged at 50g for 5 minutes to pellet the hepatocytes. To obtain NPC fraction, the filtered liver tissue digest was subjected to postperfusion digestion in KRB containing collagenase (100 U/mL), pronase (0.02%), and DNAse (0.005%) for an additional 10 minutes. After filtering and pelleting the PC fraction, the supernatant containing the crude NPC fraction was centrifuged at 1,000g for 10 minutes and the pellet resuspended in 20% iodixanol (Opti-Prep, Axis-Shield, Norton, MA), with a 17% iodixanol and Gray's balanced salt solution (GBSS) layered on top of each other according to the manufacturer's instructions. After centrifugation at 500g for 15 minutes, cells floated into the interface between 17% iodixanol, and GBSS were harvested and resuspended in GBSS. This NPC suspension was washed twice, checked for viability using trypan

blue, flash-frozen in liquid nitrogen, and kept at -80°C until use. For subsequent real time PCR, we extracted total RNA from the PC and NPC fractions using the PARIS Kit (Ambion, Austin, TX) and performed reverse transcription as described.

3.7. Laser capture microdissection

Mice were inoculated through the tail vein with 200 μL sterilized India ink diluted 1:100 in normal saline 24 hours before removal of the liver. Laser capture was performed using an Arcturus Autopix automated LCM system of the Molecular Pathology Core Laboratory at Rhode Island Hospital. Kupffer cells were identified by their inert carbon content and captured within 1 hour of cutting the sections. Approximately 500 Kupffer cells were captured from each sample on CapSure macro LCMcaps. RNA was extracted from the captured cells using a PicoPure RNA isolation kit (Arcturus, Mountain View, CA). Spin columns were eluted in 10 to 15 μL nuclease-free water or elution buffer from the kit, and RNA was protected with RNAse free DNAse 1 (Qiagen, Valencia, CA). We assessed RNA quality by a 6,000 Total RNA Picochip in an Agilent Bioanalyser, which provides qualitative evaluation down to 200 pg/μL. For subsequent real-time PCR, 50% to 100% of the entire extract was reverse transcribed with a Sensiscript RT kit (Qiagen), intended for use with less than 50 ng RNA per reaction.

3.8. Real-time PCR

Real-time quantitative PCR was performed using an iCycler iQ Multi-Color Real Time PCR Detection System (Bio-Rad, Hercules, CA). To detect UCP2, we created a reference plasmid by amplifying a 929-bp-long fragment of the mouse UCP2 gene (primers: forward, 5'-GAT CCA TAT GGT TGG TTT CAA GGC CAC-3'; reverse, 5'-ATG AAG CTT TCA GAA AGG TGC CTC CC-3') and subsequently inserting it into the pCR2.1 vector by TA cloning. Successful cloning was confirmed by sequence analysis. We used the TATA boxbinding protein (TBP) as reference gene. The full length mouse TBP gene (957 bp) was amplified (primers: forward, 5'-ATG GAC CAG AAC AAC AGC CTT C-3'; reverse: 5'-CTA TGT GGT CTT CCT GAA TCC CTT T-3') and cloned into pCR2.1. Serial dilutions of the UCP2 and TBP plasmids were used to create standard curves. Thermal cycling conditions to amplify UCP2 from samples involved 45 cycles, with denaturation at 95°C for 15 seconds, annealing at 60°C for 30 seconds and extension at 72°C for 30 seconds using 0.4 μmol/L (final concentration) each of the intron-spanning primers (forward, 5'-AGC CCT TGA CTC TCC CCT TG-3'; reverse, 5'-GCA TTG CAG ATC TCA TCA CTT TCC-3'; amplicon length, 51 bp). For TBP, the PCR reaction mix contained 0.6 μmol/L each of the intron-spanning primers (forward, 5'-ACT TCG TGC AAG AAA TGC TGA A-3'; reverse, 5'-TGT CCG TGG CTC TCT TAT TCT CA-3'; amplicon length, 75 bp). Each sample was run in duplicates and normalized using its TBP content as endogenous reference gene, and data were expressed in arbitrary units as relative abundance of UCP2 mRNA over TBP.

3.9. Treatment of rats and drug administration

The experiments were carried out with male FLF_1 (F344 X FE) hybrid rats, weighing 150-200 g. The rats were kept in a conventional laboratory environment and fed with a semi-synthetic diet (LATI, Gödöllő, Hungary) with free access to tap water. Based on the effective therapeutic doses in man, 0.5, 2 and 20 mg/kg/day fluvastatin (Lescol®, Novartis) were applied. The animals received the different doses of fluvastatin orally, either started simultaneously with the implantation for 5, 10 and 15 days or were pretreated for 21 days before the surgical procedure when we discontinued drug administration. Also, in a third group of animals, fluvastatin was given before and continued after tumor implantation. The drug was suspended in 0.5 ml corn oil and administered through a gastric tube once daily after superficial ether anaesthesia. No animal loss occurred throughout the study. The animal experiments were authorized by the Ethical Committee for Animal Research of University of Debrecen.

3.10. Tumor induction

Hepatocellular carcinoma was induced in newborn F344 inbred rats with intraperitoneal administration of 125 µg of dimethyl nitrosamine/animal (Sigma No.77561) dissolved in physiologic saline. The developed tumor was removed 5-7 months later and cancer cells were isolated from the tumor tissues under sterile conditions. The removed tissues were cut into small pieces, homogenized and filtered through a nylon mesh. The tumor cells (He/De14) were stored in liquid nitrogen. Before implantation, tumor cells were suspended in M 199 medium and diluted so that 1 µl of medium contained the appropriate number of living cells. The growth of the hepatocellular carcinoma was evaluated 5, 10 and 15 days after tumor cells were implanted under the left renal capsule.

3.11. Preparation of Gelaspon discs

In order to implant tumor cells, gelatin sponge discs (Gelaspon®, Germed, Germany) of 4 mm diameter and 1 mm thick were prepared, sterilized by ethylene oxide and were used within 1 week. Before implantation 1 µl of the cell suspension was dropped on each disc.

3.12. Surgical procedures

Rats were anesthetized by ether, and the lumbal area, previously shaven, was prepared. According to the method of Uzvölgyi et al., the left kidney was isolated and the Gelaspon disc containing the tumor cells was placed under the renal capsule. A sterile Gelaspon disc containing no tumor cells was placed under the right renal capsule as control and the wound was closed. On the 5th, 10th and 15th day after tumor implantation, the rats were anesthetized, and both kidneys were removed. The kidneys were weighed and the difference in net weight between the control and tumorous kidneys for each animal was calculated. The tumor weight did not exceed the 10 % of the total body weight of the animals.

3.13. Statistical analysis

We expressed data as mean ± SEM and performed statistical analysis with unpaired Student t test or ANOVA (one way analysis of variance) when multiple comparisons were made. Association between categorical groups was evaluated by the Fisher's exact probability, Mann-Whitney U test, and binomial exact calculations. Differences with calculated P values of less than 0.05 were regarded as significant.

Statistical calculations for the statin studies were also made by ANOVA followed by Bonferroni's t test for repeated measurements. Differences were considered statistically significant at $P < 0.05$ and data was expressed as mean ± SD.

4. RESULTS AND DISCUSSION

4.1. UCP2 deficiency affects survival, serum ALT levels, and liver injury in Jo2-treated *ob/ob* mice

Administration of low-dose Jo2 antibody caused no lethality among *ob/ob:ucp2*$^{-/-}$ mice and all but one *ob/ob:ucp2*$^{+/+}$ mouse survived by 24 hours. By contrast, all mice in both groups died within 24 hours when exposed to high-dose anti-Fas antibody. However, even within the short course of fulminant liver failure, *ob/ob:ucp2*$^{-/-}$ mice survived longer (571±81 minutes vs. 390±50 minutes, P< 0.05), indicating that UCP2 deficiency may confer partial protection against the consequences of Fas stimulation.

To assess Jo2-induced acute liver injury, we monitored serum ALT levels up to 24 hours or until the animals became moribund, whichever occurred earlier. After the administration of low-dose Jo2, ALT levels in *ob/ob:ucp2*$^{+/+}$ mice were higher at each examined time point when compared with *ob/ob:ucp2*$^{-/-}$ mice (at start: 60,8±10,1 vs. 46,1±25,7 IU/L; 2 hours later: 449,5 ± 150,0 vs. 111,5±36,8 IU/L; 12 hours later: 896,3±285,2 vs. 348,7±119,9 IU/L). As expected, treatment with high-dose Jo2 caused more rapid and severe ALT elevation, but to a lesser extent in *ob/ob:ucp2*$^{-/-}$ mice (at start: 99,1±49,8 vs. 93,8±45,9 IU/L, 1 hour later: 447,4±344,6 vs. 227,8±119,2 IU/L; 2 hours later: 2968,9±2761,9 IU/L vs. 907,4±382,3 IU/L).

Histological evaluation of acute liver damage indicated limited changes after the treatment of *ob/ob:ucp2*$^{+/+}$ and *ob/ob:ucp2*$^{-/-}$ mice with low-dose Jo2. Hematoxylin-eosin staining identified many apoptotic hepatocytes, primarily located in zone 2, more so in *ob/ob:ucp2*$^{+/+}$ than in *ob/ob:ucp2*$^{-/-}$ mice. In contrast, high-dose Jo2 treatment caused massive hemorrhagic necrosis in the livers of *ob/ob:ucp2*$^{+/+}$ mice when assessed at the time of death. Necrosis appeared less extensive, and sparing of the periportal areas was more apparent in mice with *ob/ob:ucp2*$^{-/-}$ genotype. These results correlate with the survival data and indicate that UCP2 deficiency attenuates Fas-mediated acute liver injury in ob/ob mice.

4.2. UCP2 deficiency reduces Fas-mediated liver cell death in *ob/ob* mice

To further assess the impact of UCP2 deficiency on Fas-mediated liver injury, we determined and compared the extent of hepatocellular apoptosis in different treatment groups. Importantly, we identified a small number of apoptotic hepatocytes by TUNEL assay in the livers of saline-treated animals and found that baseline apoptosis rates were significantly lower in livers of untreated *ob/ob:ucp2*$^{-/-}$ mice. Low-dose Jo2 treatment markedly increased the number of apoptotic hepatocytes, but to a lesser degree in *ob/ob:ucp2*$^{-/-}$ mice than in *ob/ob:ucp2*$^{+/+}$ mice. This finding is concordant with lower serum ALT levels seen in *ob/ob:ucp2*$^{-/-}$ mice in response to low-dose Jo2. High-dose Jo2 treatment of *ob/ob:ucp2*$^{+/+}$ mice induced dramatic changes in the appearance of liver with numerous apoptotic cells engulfed by confluent areas of necrotic hepatocytes that also stained positive by the TUNEL assay. Many liver cells within these areas displayed a diffuse staining pattern consistent with the necrotic process as opposed to the dark-staining and shrunken nuclei that are typical of apoptosis. Numerical evaluation confirmed that hepatocellular apoptosis rates in *ob/ob:ucp2*$^{+/+}$ mice are significantly higher at baseline and after low-dose Jo2 treatment when compared to *ob/ob:ucp2*$^{-/-}$ mice (baseline: 2,37±0,64 vs. 1,53±0,55 apoptosis/high power field - HPF; after low-dose Jo2: 35,40±6,07 vs. 16,18±3,72 apoptosis/HPF). Although the number of apoptotic cells in the livers of *ob/ob:ucp2*$^{-/-}$ mice treated with high-dose Jo2 was lower, this difference was not significant (101,0±22,0 vs. 54,0±10,3 apoptosis/HPF; P=0.086).

Because most liver tissue slides after high-dose Jo2 treatment displayed mixed features of apoptosis and necrosis, we assessed the extent of hepatocellular death by image analysis in which both apoptotic and necrotic cells were included, and we found that high-dose Jo2 treatment caused significantly less damage in the liver of *ob/ob:ucp2*$^{-/-}$ mice when evaluated by this method (895,13±100,75 vs. 449,62±104,47 arbitrary units).

Because apoptosis is energy-dependent and necrosis may prevail as a form of cell death in energetically compromised hepatocytes, these findings suggest that hepatocytes of *ob/ob:ucp2*$^{-/-}$ mice may retain more ATP, accounting for relatively higher fraction of cells dying through apoptosis. Nonetheless, assessment of DNA fragmentation, a hallmark of the apoptotic process, clearly showed that DNA laddering is diminished in the liver tissue of *ob/ob:ucp2*$^{-/-}$ mice when compared with *ob/ob:ucp2*$^{+/+}$ mice after treatment with both low- and high-dose Jo2. Because upregulation of Fas contributes to increased Fas-mediated liver injury in mice with diet-induced obesity, we assessed Fas expression by immunoblot analysis in livers of *ob/ob:ucp2*$^{+/+}$ and *ob/ob:ucp2*$^{-/-}$ mice and found no difference, indicating that altered Fas expression could not explain the effects of UCP2 deficiency.

4.3. UCP2 deficiency results in limited loss of hepatic ATP content in Jo2-treated *ob/ob* mice

To assess the impact of UCP2 on liver tissue energy homeostasis, we measured hepatic ATP content of *ob/ob* mice exposed to Jo2. Because UCP2 in the liver of *ob/ob* mice is expressed several

folds higher than in lean littermates, hepatocellular ATP synthesis may become impaired in *ob/ob:ucp2*$^{+/+}$ mice, leading to increased vulnerability during acute challenges. We found that hepatic ATP content in saline-treated mice was similar (*ob/ob:ucp2*$^{+/+}$ vs. *ob/ob:ucp2*$^{-/-}$ mice: 1,432±0,189 vs. 1,086±0,131 nmol/mg protein), indicating that UCP2 abundance in fatty liver does not compromise ATP synthesis under resting conditions. This is not surprising in light of the increasing evidence that ambient UCP2 has no perceptible biological effect unless activated. Interestingly, hepatic ATP content remained essentially unaltered after treatment with low-dose Jo2 (*ob/ob:ucp2*$^{+/+}$ vs. *ob/ob:ucp2*$^{-/-}$ animals: 1,090±0,303 vs. 1,652±0,349 nmol/mg protein), suggesting correction by hepatocellular homeostasis and in line with the unanimous survival of these animals. By contrast, hepatic ATP content decreased dramatically after treatment with high-dose Jo2, and UCP2 deficiency had a significant impact on this process. Thus, residual hepatic ATP content remained approximately threefold higher in the livers of moribund *ob/ob:ucp2*$^{-/-}$ mice (*ob/ob:ucp2*$^{+/+}$ vs. *ob/ob:ucp2*$^{-/-}$ mice: 0,139±0,024 vs. 0,448±0,167 nmol/mg protein). These results indicate that liver ATP stores are better preserved in the absence of UCP2 and support the notion that increased UCP2 expression contributes to increased vulnerability of fatty liver under certain conditions.

4.4. UCP2 deficiency and oxidative stress in Fas-mediated liver injury of *ob/ob* mice

Because regulation of mitochondrial ROS production as a major function of UCP2 is increasingly accepted, we analyzed the effect of UCP2 deficiency on oxidative stress in livers of Jo2-treated *ob/ob* mice. As predicted, increasing doses of Jo2 induced significant elevation in the degree of lipid peroxidation assessed by accumulation of MDA in the liver of *ob/ob:ucp2*$^{+/+}$ and *ob/ob:ucp2*$^{-/-}$ mice (*ob/ob:ucp2*$^{+/+}$ vs. *ob/ob:ucp2*$^{-/-}$ mice; saline-treated: 0,405±0,031 vs. 0,486±0,080 nmol/mg protein; after low-dose Jo2: 0,688±0,191 vs. 0,775±0,090 nmol/mg protein, after high-dose Jo2: 0,903±0,081 vs. 0,900±0,140 nmol/mg protein). Surprisingly, however, UCP2 deficiency had no discernible impact on liver tissue MDA levels, suggesting that altered oxidative stress is not a major modulator of Fas-mediated liver injury in *ob/ob:ucp2*$^{-/-}$ mice. This finding is at variance with reports in which reduced presence or absence of UCP2 led to increased oxidative stress in a variety of cells under various conditions. Therefore, we addressed this problem in subsequent experiments.

4.5. Differential changes in UCP2 expression of hepatocytes and Kupffer cells in *ob/ob* mice

Liver tissue expresses the rather ubiquitous UCP2 mainly in Kupffer cells and has little or no UCP2 present in hepatocytes under healthy conditions. This pattern of cell-specific UCP2 expression appears to change in fatty liver associated with diet-induced or genetically determined obesity in which hepatocytes display markedly increased amounts of UCP2 mRNA and protein. UCP2 expression is decreased in peritoneal macrophages of obese rodents, although whether a similar reduction of UCP2 occurs in Kupffer cells associated with obesity and fatty liver remains unknown.

We speculated that downregulation of UCP2 expression in Kupffer cells of *ob/ob* mice could provide an explanation for the lacking effect of UCP2 deficiency on liver tissue oxidative stress induced by Jo2. We reasoned that UCP2 ablation might have little further impact on the function of Kupffer cells, a major source of ROS production in the liver, if these cells have an already diminished presence of UCP2 in *ob/ob* mice. To determine whether changing UCP2 expression follows a cell-specific pattern in fatty liver, we obtained fractions of parenchymal cells (PC) and non-parenchymal cells (NPC) by in situ liver perfusion of UCP2-competent ob/ob mice and their wild-type littermates *(wt/wt)* and compared UCP2 expression in these cellular fractions. Analysis of UCP2 expression in the PC fraction showed several-fold higher UCP2 mRNA (*wt/wt* vs. *ob/ob*: 4,80±0,965 vs. 15,463±2,516), in line with previous observations in which exposure of primary hepatocytes to large amounts of fatty acids caused UCP2 upregulation. By contrast, UCP2 mRNA levels were significantly lower in the NPC fraction obtained from *ob/ob* livers when compared with lean controls (*wt/wt* vs. *ob/ob*: 89,27±22,12 vs. 39,26±21,34). Because the NPC fraction also contains non-Kupffer cells, such as sinusoid endothelial cells and stellate cells in which the presence or absence of UCP2 has not been reported, we also analyzed UCP2 expression in Kupffer cells identified by India ink phagocytosis and collected by laser capture microdissection. To avoid the effect of potential contamination from non-Kupffer cells, we corrected UCP2 mRNA to the transcript levels of Kupffer cell-specific CD68. Similar to the crude NPC fraction, UCP2 expression in Kupffer cells was significantly reduced in *ob/ob* mice when compared with lean control (*wt/wt* vs. *ob/ob*: 28,69±7,43 vs. 11,71±2,82).

4.6. Toward a model of cell-specific modulation of UCP2 in fatty liver

Our results indicate that downregulation of UCP2 previously demonstrated in peritoneal macrophages of *ob/ob* mice28 also occurs in Kupffer cells of these animals. Although the sample size and low UCP2 protein abundance did not allow us to conduct Western blot analysis, the changes seen in Kupffer cell UCP2 mRNA levels associated with fatty liver are potentially very important and reported for the first time to our knowledge. In vitro inhibition of UCP2 in rat liver NPC fractions results in increased ROS production, a finding consistent with Kupffer cell activation. Downregulation of UCP2 in Kupffer cells, rather than its upregulation in hepatocytes, may be a key contributor to increased oxidative stress in fatty liver of *ob/ob* mice. This process, however, may not escalate in *ob/ob:ucp2*$^{-/-}$ mice if the impact of UCP2 ablation is negligible on Kupffer cells with already diminished UCP2 expression. Accordingly, UCP2 deficiency has no significant effect on liver tissue MDA content in Jo2-treated *ob/ob* mice. By contrast, the effect of UCP2 ablation is considerable in fatty hepatocytes, where UCP2 deficiency appears to spare ATP stores and attenuate sensitivity of *ob/ob:ucp2*$^{-/-}$ mice to Fas-mediated injury. Altogether, our findings obtained in *ob/ob* mice are best explained with a model in which cell-specific regulatory changes of UCP2 expression have their separate contribution to the pathogenesis of fatty liver. Thus, diminished UCP2 in Kupffer cells would primarily increase ROS output and promote oxidative stress, whereas excess UCP2 in hepatocytes

would primarily impair ATP production and hepatocellular energy balance. Because UCP2 requires specific activators, its amplified presence in fatty hepatocytes may only manifest on acute challenges. When this occurs, however, fatty hepatocytes may benefit from the lack of UCP2 as seen in Jo2-treated *ob/ob:ucp2*$^{-/-}$ mice. Whether other animal models of fatty liver exhibit the paradigm of cell-specific transcriptional regulation of UCP2 as described in *ob/ob* mice remains unclear. Little is known about hepatic UCP2 expression in human NAFLD and in these experimental conditions. Based on our findings, however, the therapeutic value of stimulating UCP2 expression in fatty liver remains questionable unless it is specifically directed to prevent decreased UCP2 function in Kupffer cells. Although the latter seems a desirable goal, the negative transcriptional regulation of UCP2 in macrophages, including Kupffer cells, awaits elucidation.

4.7 Determining the optimal conditions of tumor implantation

Implantation of tumor pieces and isolated tumor cells under the renal capsule is a commonly used method. However, evaluation procedures do not always provide a precise analysis of tumor development. The advantage of Gelaspon discs is that the gelatin reabsorbs the cells attached to each other and to the renal collagen fibers. Therefore, the cell aggregate does not disturb renal microcirculation and tissue metabolism. Also, this experimental system is inexpensive and useful for quantitative evaluation of chemoterapeutic and chemopreventive drugs.

In the first series of experiments, the optimal number of implanted cells and the optimal time for the evaluation of hepatocellular carcinoma development were determined. 10^5, 10^6 or 10^7 hepatocellular carcinoma cells were placed under the renal capsule of untreated rats and the tumor development was evaluated at 5, 10 and 15 days after surgical procedure. Tumor weight can already be detected on the 5th day after inoculation, and it was found to have maximal values 15 days after tumor implantation. Prolonged periods of tumor growth were not studied, because between 15 and 25 days the death of animals would have had to be taken into consideration. Based on these preliminary results tumor development was determined on the 5th, 10th and 15th day after the surgical procedure. On the other hand, tumor growth after the implantation of 10^5 carcinoma cells was poor (5th day: 0,119±0,02; 10th day: 0,456±0,07; 15th day: 3,789±0,56 g/100g body weight-BW), while tumor development when implanting 10^6 hepatocellular carcinoma cells was not significantly enhanced by the use of 10^7 tumor cells (5th day: 0,455±0,07 vs. 0,553±0,11 g/100g BW; p=0,0965; 10th day: 5,882±1,05 vs. 6,117±1,15 g/100g BW; p=0,2612; 15th day: 8,673±1,55 vs. 9,823±1,86 g/100g BW; p=0,0524). Therefore, fluvastatin treatment was carried out on rats inoculated with 10^6 hepatocellular carcinoma cells.

4.8 Effect of fluvastatin treatment on tumor growth when starting simutaneously with tumor implantation

Rats were treated *per os* with 0.5, 2 and 20 mg/kg/day doses of fluvastatin from the day of tumor implantation to the day of tumor growth evaluation. 0.5 mg/kg/day dose did not arrest tumor growth (tumor weigths of control group on the 5th day: 0,55±0,1; 10th day: 6,54±1,1; 15th day: 7,78±1,5 g/100g BW vs. low-dose fluvastatin treated rats on 5th day: 0,60±0,1; 10th day: 5,79±1,2; 15th day: 7,56±1,6 g/100g BW), whereas treatment with 2 mg/kg/day dose resulted in a significant anticancer effect, although, this anticancer effect could only be detected after 15 days (5th day: 0,58±0,1; 10th day: 6,11±1,2; 15th day: 5,87±1,1 g/100g BW; $p<0,001$). In contrast with these, the antitumor effect of 20 mg/kg/day simultaneous fluvastatin treatment was significant after both 10 and 15 days (5th day: 0,62±0,1; 10th day: 5,21±1,1; $p<0,01$; 15th day: 4,88±0,9 g/100g BW; $p<0,001$).

4.9. Effect of fluvastatin pretreatment of tumor growth

To further determine the chemopreventive effect of fluvastatin, rats were pretreated for 21 days prior to tumor implantation. Our results suggest that under these conditions, the drug has no chemopreventive effect on the tumor growth in the applied concentrations (tumor weights of control group on the 5th day: 0,79±0,1; 10th day: 5,68±1,1; 15th day: 8,67±1,7 g/100g BW; tumor weights of rats treated with 0,5 mg/ttkg fluvastatin on the 5th day: 0,80±0,2; 10th day: 4,68±1,0; 15th day: 8,56±1,8 g/100 g BW; tumor weights of rats treated with 2 mg/ttkg fluvastatin on the 5th day: 0,83±0,2; 10th day: 5,87±1,2; 15th day: 8,88±1,8 g/100 g BW; tumor weights of rats treated with 20 mg/ttkg fluvastatin on the 5th day: 0,77±0,1; 10th day: 4,67±1,1; 15th day: 8,12±1,6 g/100 g BW).

4.10. Effect of combined pre- and post-implantational administration of fluvastatin on hepatocellular tumor growth

In a third group of animals rats were pretreated with fluvastatin before tumor implantation and the drug administration was continued for different periods of time. We observed the most intense anticancer effect in this group: fluvastatin had a significant inhibitory effect on the growth of the implanted hepatocellular tumor after 15 days when given in 0.5 mg/kg dose (tumor weights of control group on the 5th day: 0,79±0,1; 10th day: 5,72±1,1; 15th dayn: 8,24±1,7 g/100g BW vs. tumor weights of rats treated with 0,5 mg/kg fluvastatin on the 5th day: 0,69±0,1; 10th day: 5,31±1,2; 15th day: 7,21±1,5 g/100 g BW; $p<0,001$). Fluvastatin also showed a significant inhibitory effect on tumor growth in all examined time intervals when administered in 2 and 20 mg/kg daily doses (tumor weights of rats treated with 2 mg/kg fluvastatin on the 5th day: 0,61±0,1; 10th day: 4,46±0,8; 15th day: 5,56±1,1 g/100 g BW, $p<0,05$, $p<0,01$, $p<0,001$, respectively, when compared to control group; tumor weights of rats treated with 20 mg/kg fluvastatin on the 5th day: 0,44±0,1; 10th day: 3,53±0,6; 15th day: 2,69±0,5 g/100 g BW, $p<0,01$, $p<0,01$, $p<0,001$, respectively, when compared to control group).

Our results show that oral administration of fluvastatin significantly reduced growth of implanted hepatocellular cancer cells. We observed its inhibitory effect in higher doses when drug administration was started simultaneously with tumor implantation; and this effect was enhanced when fluvastatin was given to the animals prior to and continued after tumor implantation. We could detect significant anticancer effects even after smaller doses of fluvastatin. Based upon our data, fluvastatin administration can be beneficial in treatment of human malignancies; however, further studies needed to prove its efficiency and safety.

5. SUMMARY

Non-alcoholic fatty liver and subsequent insulin resistency are important complications of obesity. NAFLD is vulnerable to conditions that compromise hepatocellular energy homeostasis. Lipid-laden hepatocytes highly express uncoupling protein-2, which – by mediating the proton leak – competes with the cells' ATP synthesis and modulates the generation of reactive oxygen species. However, the link between UCP2 expression and susceptibility of fatty liver to acute injury is still unclear. We asked whether absence of UCP2 is beneficial for leptin deficient *ob/ob* mice when challenged with Fas-mediated cell destruction and subsequent acute liver injury. *Ob/ob* mice deficient for UCP2 *(ob/ob:ucp2$^{-/-}$)* and UCP2-competent littermates *(ob/ob:ucp2$^{+/+}$)* received a single dose of agonistic anti-Fas antibody (Jo2) intraperitoneally. Low-dose Jo2 (0,15 mg/ttkg) caused less ALT elevation and lower apoptosis rates in *ob/ob:ucp2$^{-/-}$* mice. High-dose Jo2 (0,4 mg/ttkg) proved uniformly fatal in 24 hours; however, *ob/ob:ucp2$^{-/-}$* mice survived longer with less depletion of hepatic ATP stores, indicating that fatty hepatocytes may benefit from ablation of UCP2 during Fas-mediated acute liver injury. Although UCP2 reportedly controls mitochondrial generation of ROS, we could not detect significant difference in MDA levels of tissue lysates from the different genotypes. This finding prompted us to determine UCP2 expression in Kupffer cells, a major source of intrahepatic oxidative stress. UCP2 expression was found diminished in Kupffer cells of untreated *ob/ob:ucp2$^{+/+}$* mice, contributing to increased oxidative stress and limiting the impact of UCP2 ablation. Therefore, UCP2 abundance in fatty liver exacerbates Fas-mediated cell destruction by compromising ATP stores and diminished expression of UCP2 found in Kupffer cells results in persistent oxidative stress. Our data emphasize the cell-specific therapeutic approach when considering the enhancement of mitochondrial uncoupling in fatty liver disease.

Fluvastatin is a widely used drug in treatment of hyperlipidemia which is commonly associated with obesity. However, its chemopreventive effect on *in vivo* tumor development has not been studied yet. Using Gelaspon sponge discs we implanted hepatocellular cancer cells under the renal capsules of rats. The animals received different doses of fluvastatin orally, either started simultaneously with the implantation or were pretreated only before the surgical procedure. Also,

fluvastatin was administered before and continued after the tumor implantation in a third group of animals. The drug showed no significant impact on cancer development when given only before implantation; while the anticancer effect was detectable in higher doses of simultaneous administration. Additionally, chemopreventive fluvastatin treatment continued after tumor implantation demonstrated the most intense anticancer effect. Our results draw the attention to the beneficial effect of fluvastatin inhibiting *in vivo* hepatocellular cancer development.

6. RESEARCH COMMUNICATIONS

Peer-reviewed publications founding the Ph.D. thesis:

Fülöp P, Derdák Z, Sheets A, Sabo E, Berthiaume EP, Resnick MB, Wands JR, Paragh G, Baffy G. Lack of UCP2 reduces Fas-mediated liver injury in ob/ob mice and reveals importance of cell-specific UCP2 expression. *Hepatology* 2006; 44(3):592-601

IF: 9,792

Paragh G, Kertai P, Kovács P, Paragh G Jr, **Fülöp P**, Fóris G. HMG CoA reductase inhibitor fluvastatin arrests the development of implanted hepatocarcinoma in rats. *Anticancer Res* 2003; 23(5A):3949-3954

IF: 1,347

Other peer-reviewed publications:

Paragh G, Seres I, Balogh Z, Katona E, **Fülöp P**, Kárpáti I, Mátyus J, Kakuk G. Szérum paraoxonáz aktivitás vizsgálata krónikus urémiás betegekben. *Hypertonia és Nephrologia* 1999; 3(2):106-109

Paragh G, Seres I, Balogh Z, Harangi M, Katona E, **Fülöp P**, Kakuk G. A szimvasztatin hatása a szérum lipid szintekre és a paraoxonáz aktivitásra. *Magyar Belorv Arch* 1999; 3:255-258

Seres I, Varga Z, Balogh Z, Harangi M, **Fülöp P**, Kakuk G, Paragh G. Szérum paraoxonáz aktivitás és E-vitamin szintek hypercholesterolaemiás betegekben. *Magyar Belorv Arch* 2000; 53:115-117

Balogh Z, **Fülöp P**, Seres I, Harangi M, Katona E, Kosztáczky B, Paragh G. Effects of simvastatin on serum paraoxonase activity. *Clin Drug Invest* 2001; 21:505-510

IF: 0,846

Audikovszky M, Pados G, Seres I, Harangi M, **Fülöp P**, Katona E, Winkler G, Paragh G. Obes betegek lipidprofiljának és paraoxonáz aktivitásának változása orlistat kezelést követően. *Orv Hetil* 2001; 142(50):2779-2783

Illyés L, Seres I, **Fülöp P**, Paragh G. Revaszkularizációs műtéten átesett betegek szérum paraoxonáz aktivitása. *Cardiologia Hungarica* 2003; 33:11-15

Horimoto M, **Fülöp P**, Derdák Z, Wands JR, Baffy G. Uncoupling protein-2 deficiency promotes oxidant stress and delays liver regeneration in mice. *Hepatology* 2004;39(2):386-92

IF: 10,416

Paragh G, Fóris G, Paragh G Jr, Seres I, Karányi Z, **Fülöp P**, Balogh Z, Kosztáczky B, Teichmann F, Kertai P. Different anticancer effects of fluvastatin on primary hepatocellular tumors and metastases in rats. *Cancer Lett* 2005; 222(1):17-22

IF: 3,049

Derdák Z, **Fülöp P**, Sabo E, Tavares R, Berthiaume EP, Resnick MB, Paragh G, Wands JR, Baffy G. Enhanced colon tumor induction in uncoupling protein-2 deficient mice is associated with NF-kappaB activation and oxidative stress. *Carcinogenesis* 2006; 27(5):956-961

IF: 5,108

Kosztáczky B, Fóris G, Seres I, Balogh Z, **Fülöp P**, Koncsos P, Paragh G. Neuropeptides induced a pronounced and statin-sensitive dysregulation of mevalone cycle in human monocytes of patients with hypercholesterolemia. *Neuropeptides* 2006; 40(5):309-316

IF: 2,155

Seres I, Fóris G, Varga Z, Kosztáczky B, Kassai A, Balogh Z, **Fülöp P,** Paragh G. The association between angiotensin II-induced free radical generation and membrane fluidity in neutrophils of patients with metabolic syndrome. *J Membr Biol* 2006; 214(1-2): 91-98

IF: 2,112

Audikovszky M, Pados G, Seres I, Harangi M, **Fülöp P**, Katona E, Illyés L, Winkler G, Katona ÉM, Paragh G. Orlistat increases serum paraoxonase activity in obese patients. *Nutr Metab Cardiovasc Dis* 2007; 17(4) 268-273

IF: 1,482

Cumulative impact factor of the *in extenso* publications: 36, 307

Abstracts of peer-reviewed oral and poster publications:

Tóth A, **Fülöp P**, Csortos C, Gergely P, Erdõdi F. Purification and identification of protein phosphatase with type-specific antibodies. *1st Scientific Conference of the Hungarian Biochemical Society - Molecular Biology Group,* Seregélyes, Hungary, 1996

Katona E, Seres I, Balogh Z, **Fülöp P**, Kakuk G, Paragh G. Changes in the serum paraoxonase activity of patients with chronic kidney failure. *12st Conference of the Hungarian Atherosclerosis Society,* Sopron, Hungary, 1998

Fülöp P, Katona E, Seres I, Balogh Z, Harangi M, Paragh G. The impact of simvastatin therapy on serum paraoxonase activity. *12st Conference of the Hungarian Atherosclerosis Society,* Sopron, Hungary, 1998

Katona E, Seres I, Balogh Z, **Fülöp P**, Kakuk G, Paragh G. Changes in serum paraoxonase activity in hemodialysed patients. *3rd Scientific Forum of the Frigyes Korányi Special College of the Semmelweis University Medical School,* Budapest, Hungary, 1999 (1st prize winner)

Seres I, Varga Z, Balogh Z, Harangi M, **Fülöp P**, Kakuk G, Paragh G. Changes in serum paraoxonase activity and vitamin E levels of hemodialysed patients. *13rd Conference of the Hungarian Atherosclerosis Society,* Sopron, Hungary, 2000

Seres I, Varga Z, Balogh Z, Harangi M, **Fülöp P**, Kakuk G, Paragh G. Paraoxonase activity and alpha-tocopherol levels in hypercholesterolemic patients. *Atherosclerosis* 2000; 146(Suppl):35

Fülöp P, Resnick M, Wands JR, Baffy G. UCP2 affects fasting-induced steatosis and metabolic parameters in lean and obese mice. *Hepatology* 2002; 36:486A (AASLD President's Choice Poster)

Horimoto M, **Fülöp P**, Wands JR, Baffy G. Liver regeneration is delayed after partial hepatectomy in mice deficient for uncoupling protein-2. *Gastroenterology* 2003; 124(4 Suppl 1):A722

Monti NA, **Fülöp P**, Resnick M, Wands JR, Baffy G. Uncoupling protein-2 modulates crypt cell apoptosis rate in the colon of mice fed with high-fat diet. *Gastroenterology* 2003; 124(4 Suppl 1):A261

Fülöp P, Resnick M, Wands JR, Baffy G. Fas-mediated liver injury in ob/ob mice is attenuated in the absence of uncoupling protein-2. *Gastroenterology* 2003; 124(4 Suppl 1):A757 (AGA Poster of Distinction)

Baffy G, **Fülöp P**, Wands JR, Horimoto M. Modulation of oxidant production and cell cycle activity by uncoupling protein-2 in regenerating mouse liver. *XII Falk Liver Week*, Freiburg, Germany, 2003 (3rd prize winner)

Horimoto M, Derdák Z, **Fülöp P**, Wands JR, Baffy G. Uncoupling protein-2 deficiency alters cell cycle protein expression in regenerating mouse liver. *Hepatology* 2003; 38:235A

Fülöp P, Derdák Z, Resnick M, Wands JR, Paragh G, Baffy G. Impact of mitochondrial UCP2 on fasting-induced steaosis. *15th Conference of the Hungarian Atherosclerosis Society,* Sopron, Hungary, 2004

Fülöp P, Sheets A, Derdák Z, Resnick M, Paragh G, Wands JR, Baffy G. Studies on the effects of UCP2 on hepatic lipid metabolism in fasting. *3rd Conference of the Hungarian Society on the Study of Free Radicals,* Debrecen, Hungary, 2005

Derdák Z, **Fülöp P**, Konkin A, Resnick A, Wands JR, Baffy G. Enhanced colon tumor induction by azoxymethane in mice deficient for UCP2. *Uncoupling proteins: Current status and therapeutic prospects,* Madrid, Spain, 2005

Derdák Z, **Fülöp P**, Konkin A, Resnick A, Wands JR, Paragh G, Baffy G. Azoxymethane is more tumorigenic in the colon of UCP2-deficient mice. *Gastroenterology* 2005; 125(4 Suppl 1): A176